INORGANIC CHEMISTRY FRONTIERS

RESEARCH ARTICLE

View Article Online
View Journal | View Issue

Cite this: *Inorg. Chem. Front.*, 2023, **10**, 1795

New reticular chemistry of pillared rare-earth kgd supermolecular building layer frameworks with ethane-trapping property†

Hong-Xin Li, Han Fang, Yu-Feng Zhang, Zong-Hui Zhang and Dong-Xu Xue *

Received 16th January 2023,
Accepted 7th February 2023

DOI: 10.1039/d3qi00103b

rsc.li/frontiers-inorganic

The industrial demand for ethylene is increasing, efficient purification of ethylene from ethane is of significant importance but challenging. Pillar-layered metal–organic frameworks (MOFs) have aroused extensive attention due to their application potential in gas separation, storage and catalysis, *etc.* Herein, five pillar-layered rare-earth (RE)-MOFs based on rare **kgd** supermolecular building layers (SBLs) were successfully prepared under solvothermal conditions by means of $Tb(NO_3)_3{\cdot}6H_2O$ as the metal source, single tritopic H_3NTB (4,4′,4″-nitrilotribenzoic acid) or mixed H_3NTB, with a series of ditopic ligands with distinct length as the bridge linkers. Single crystal structure analyses show that three types of pillar-layered RE-MOFs were isolated due to the difference of pillars between the exclusive **kgd** SBLs, *i.e.*, **trk**, **zma** and **tpk** topological networks. The N_2 isotherms exhibit that the first four MOFs feature microporous characteristics. Furthermore, the single component of C_2H_6, C_2H_4, C_2H_2 and CO_2 sorption isotherms show that the four materials exhibit reverse C_2H_6/C_2H_4 separation as well as C_2H_2-selective adsorption for a C_2H_2/CO_2 mixture. Among them, Tb-NTB-1,4-NDC displays the best separation potential as revealed by ideal adsorption solution theory and dynamic column breakthrough experiments.

Introduction

Ethylene is an important basic raw material in petrochemical production, which is widely used in the synthesis of polyethylene materials and other high value organic chemicals. By 2023, its global annual production capacity will exceed 200 million tons, and will maintain an annual growth trend of about 5%,[1–3] occupying a very important position in the national economy. Ethylene production is regarded as one of the most important indicators to measure the development level of the petrochemical industry in a country. At present, ethylene is mainly obtained by the stream cracking of naphtha and dehydrogenation of ethane in the petrochemical industry. Ethylene products obtained in this way contain ethane impurities, which affect the further application of ethylene (the purity requirement of ethylene in practical applications is not lower than 99.95%).[4,5] In order to obtain C_2H_4 with high purity, the ethane impurity in the ethylene product must be removed first. However, it is difficult to separate C_2H_4/C_2H_6 because of their similar boiling points and molecular size.[6] Industrial separation is mainly based on low temperature and high-pressure distillation. Ethylene is usually obtained under 23 bar and 248 K distillation column, 120–180 trays and high reflux ratio, which consumes a large amount of energy (7 GJ t^{-1}).[7,8] It was estimated that the separation and purification of ethylene and propylene accounts for 0.3% of global energy consumption.[9,10] Because of this, it is vital to find an alternative ethylene/ethane separation technology with low energy consumption and high efficiency. In recent years, adsorptive separation has been regarded as a very promising separation method. The key to this technology is to research and develop new adsorbents with good separation performance.

Metal–organic frameworks (MOFs) are a new class of crystalline porous materials, which have the advantages of mild synthesis conditions, good crystallinity, diverse structures, controllable pore size and modifiable pore surface, *etc.*[11] Therefore, MOF materials are ideal platforms to investigate the relationship between structure and properties. For instance, MOF materials have exhibited great potential for ethylene/ethane separation.[12–15]

Regarding whether the adsorbent preferentially captures C_2H_4 or C_2H_6, MOFs can be divided into two types. One type is C_2H_4-selective MOFs which adsorb C_2H_4 preferentially. The design of these MOFs is according to the larger quadrupole

Key Laboratory of Applied Surface and Colloid Chemistry, Ministry of Education, Xi'an Key Laboratory of Organometallic Material Chemistry, School of Chemistry & Chemical Engineering, Shaanxi Normal University, Xi'an 710062, China.
E-mail: xuedx@snnu.edu.cn

† Electronic supplementary information (ESI) available. CCDC 2235992–2235996. For ESI and crystallographic data in CIF or other electronic format see DOI: https://doi.org/10.1039/d3qi00103b

moment of C_2H_4 and the presence of π electrons, which make coordinating to metals possible, such as, HKUST-1,[16–18] M-MOF-74 [19–21] and Cu^I@UiO-66-$(COOH)_2$,[22] *etc.* C_2H_4-selective MOFs are easier to design directly and possess higher selectivity, but the separations based on C_2H_4-selective MOFs have two main drawbacks: (1) there is competitive adsorption between water vapor and C_2H_4, which results in reduced C_2H_4 adsorption sites in the framework; (2) in the separation process, although C_2H_4 is adsorbed, a small amount of C_2H_6 impurity still exists in the adsorbent due to co-adsorption, and additional adsorption–desorption procedures are needed for high purity C_2H_4. In order to meet the production purity requirements (≥99.95%) of C_2H_4, at least four cycles of adsorption–desorption are inevitable, which not only increases the cost and time of separation, but also reduces the productivity of C_2H_4. The other type is C_2H_6-selective MOFs that adsorb C_2H_6 preferentially. These MOFs mainly rely on the dispersion and induction forces because ethane has a higher polarizability than ethylene, for example, $Cu(Qc)_2$,[23] FJI-H11-Me,[24] MFM-300 (In),[25] MUF-15,[26] NKMOF-8-Br/Me,[27] *etc.* The separation based on C_2H_6-selective MOFs can obtain C_2H_4 at the outlet in one step without additional adsorption–desorption process, which can save energy and cost. Therefore, the design and synthesis of C_2H_6-selective MOFs is of great practical significance for real industrial separation.

To systematically research the effects of pore size and pore surface environment on the separation performance of C_2H_6/C_2H_4, it is necessary to select an appropriate MOF system. Pillar-layered MOFs are ideal platforms, because it is possible to fine-tune the pore size and surface of the MOF by changing the pillar, while simultaneously preserving the two-dimensional (2D) layer. Currently, there are three main methods to construct pillar-layered MOFs: axial-to-axial (A–A), axial-to-ligand (A–L) and ligand-to-ligand (L–L) that differ in the connection modes of pillars supporting 2D layers.[28] Compared with A–L and L–L approaches involving complicated organic synthesis, A–A ones based on mixed ligands are more practical. To facilitate the rational design and construction of pillar-layered MOFs, Eddaoudi *et al.* proposed a supermolecular building layers (SBLs) strategy by deconstructing pillar-layered MOF structures into 2D layers and pillars in 2011.[29] This is because there are only five edge-transitive SBLs, *i.e.*, **sql**, **kgm**, **hcb**, **hex** and **kgd**, which are a prerequisite for reticular chemistry. Interestingly, except **kgd**, the other four types of 2D net are frequently observed in pillar-layered MOFs.[28,30,31] This is most probably due to the complex **kgd** constitution composed of triangle and hexagonal types of nodes in comparison with other 2D nets. According to the literature, most reported pillar-layered MOFs were assembled from transition metal ions.[28] In contrast, rare-earth (RE) based ones are rarely documented. We are interested in the design and synthesis of RE-MOFs. With the aid of 2-fluorobenzoic acid (2-FBA), hexa/nonanuclear RE clusters can be generated *in situ*.[32–38] Since a cuboctahedral hexanuclear cluster can be split into the **kgd**-required hexagon and trigonal antiprism, pillar-layered MOFs based on **kgd** SBLs could be speculated from RE ions.

Based on the above findings and consideration, herein, a sole tritopic linker, H_3NTB (4,4′,4″-nitrilotribenzoic acid), or a mix with a series of linear ditopic linkers of H_2BDC (1,4-benzenedicarboxylic acid)/1,4-H_2NDC (1,4-naphthalenedicarboxylic acid)/H_2DTTDC (dithieno[3,2-*b*:2′,3′-*d*] thiophene-2,6-dicarboxylic acid)/H_2OBDC (4,4′-(oxalylbis(azanediyl))dibenzoic acid) were thoroughly selected and reacted with Tb$(NO_3)_3$·$6H_2O$ to isolate five pillar-layered RE-MOFs of Tb-NTB-HNTB/BDC/1,4-NDC/DTTDC/OBDC that exclusively possess **kgd** SBLs. Three distinct topological nets were identified, *i.e.*, **trk**, **zma**, and **tpk**. Subsequently, sorption studies were systematically investigated. The results reveal that four of them exhibit microporous features and an inert pore surface. Thus, these materials show exciting ethane-trapping properties, with Tb-NTB-1,4-NDC possessing the highest uptake and selectivity capacity for C_2H_6/C_2H_4 and C_2H_2/CO_2. The separation performances were further validated by dynamic column breakthrough tests.

Results and discussion

Structure analysis

Indeed, colourless polyhedral-shaped single crystals of Tb-NTB-HNTB, formulated as $[(CH_3)_2NH_2]_2[Tb_6(\mu_3\text{-}F)_8(NTB)_2(HNTB)_2(OH)_2(H_2O)_8]\cdot x$(solvent), were obtained by solvothermal reaction of Tb$(NO_3)_3$·$6H_2O$ with H_3NTB in *N*,*N*-dimethylformamide (DMF) in the presence of 2-FBA at 115 °C. Single-crystal X-ray diffraction (SCXRD) analysis revealed that Tb-NTB-HNTB crystallizes in the monoclinic *C*2/*m* space group with a = 18.018 Å, b = 31.261 Å, c = 17.687 Å, β = 111.8°, V = 9253 $Å^3$. In Tb-NTB-HNTB, the popular hexanuclear cluster was formed with rare C_{2h} symmetrical MBB of $[Tb_6(\mu_3\text{-}F)_8(O_2C\text{–})_{10}(OH)_2(H_2O)_8]$. Differently and interestingly, the organic linker in Tb-NTB-HNTB exhibits two symmetries, *i.e.*, fully deprotonated NTB^{3-} with C_3 symmetry and one carboxylate protonated $HNTB^{2-}$ with C_1 symmetry. Subsequently, each inorganic molecular building block (MBB) connects six fully deprotonated NTB^{3-} ligands, and each fully deprotonated NTB^{3-} ligand connects three MBBs, which then construct an SBL. Finally, neighbouring layers are bridged by the incompletely deprotonated $HNTB^{2-}$ pillars *via* doubly-crosslinked mode, forming a 3-periodic pillar-layered RE-MOF associated with two types of rhombic channels (the aperture sizes are 4.00 × 7.72 $Å^2$ and 3.27 × 16.46 $Å^2$, respectively) (Fig. 1 and S4†).

To further pinpoint the topology and the two types of symmetrical ligands in Tb-NTB-HNTB MOF, the merged-net approach was employed to describe the structure.[39] Interestingly, the MOF can be deconstructed into an underlying (3,6)-c **kgd** net and an unprecedented one-dimensional chain named **trc** net (Fig. 1). It is noteworthy that the **trc** net is assembled from two different rectangle SBUs, which have never been independently reported in a known one-dimensional chain structure, resulting in the unique (3,5)-c **trk**-MOF herein (**tr** from **trc** and **k** from **kgd**). In addition, if the in-

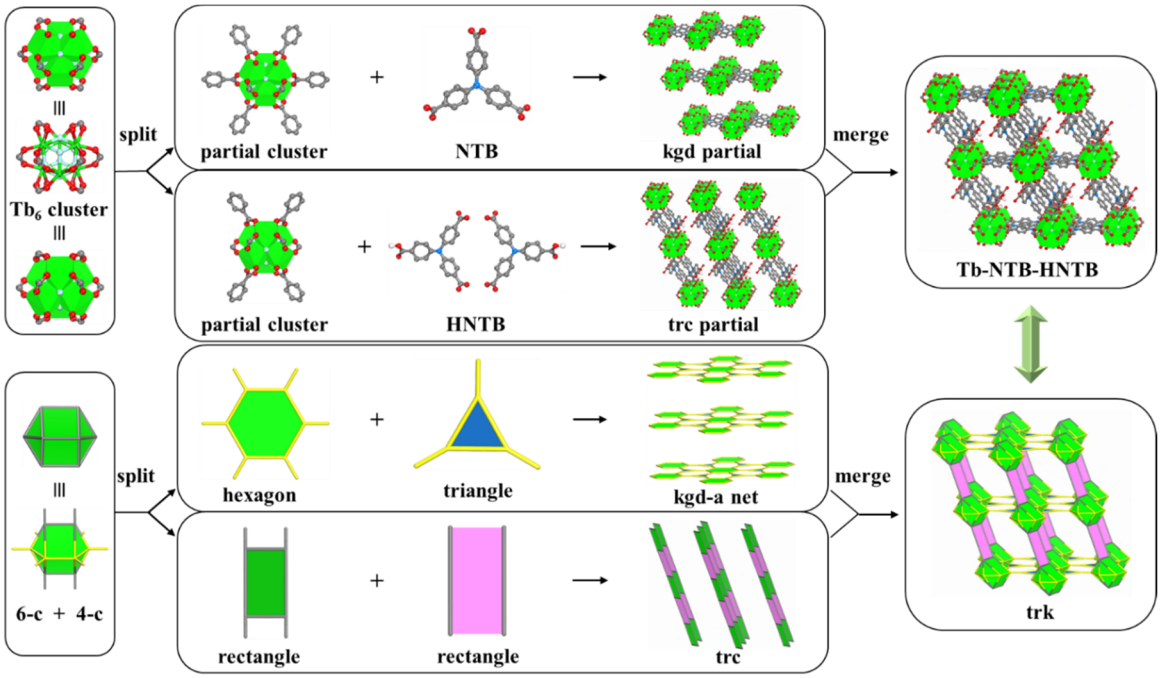

Fig. 1 Schematic representation showing the assembly of Tb-NTB-HNTB. Top: The frameworks of **kgd** and **trc** are combined to form Tb-NTB-HNTB; bottom: **kgd-a** and **trc** nets are merged to form a **trk** network. Tb = green, C = gray, H = white, N = blue, O = red and F = cyan.

organic MBBs are considered as 8-c nodes, six fully deprotonated NTB ligands are simplified to 3-c nodes, and each doubly crosslinked HNTB ligand is regarded as a connecting rod, Tb-NTB-HNTB is also considered as a (3,8)-c network with **tfz** topology (Fig. S5†).

So far, the first **kgd** SBL based pillar-layered RE-MOF was successfully constructed by means of a sole NTB linker. Considering the bulkiness of the HNTB pillar and connectivity of unsaturated MBBs in Tb-NTB-HNTB, it is possible to deduce that substituting HNTB by linear dicarboxylate linkers could produce other types of pillar-layered MOFs (Fig. S6†). Subsequently, mixing H_3NTB with a series of dicarboxylic acids, reacted with $Tb(NO_3)_3{\cdot}6H_2O$ in the presence of 2-FBA, provided four new pillar-layered RE-MOFs, namely Tb-NTB-BDC, Tb-NTB-1,4-NDC, Tb-NTB-DTTDC, and Tb-NTB-OBDC, which were all successfully isolated.

Since Tb-NTB-BDC, Tb-NTB-1,4-NDC, and Tb-NTB-DTTDC are isoreticular, Tb-NTB-BDC is taken as an example to analyse the single crystal structure. SCXRD and ^{19}F NMR [40] (Fig. S1†) analysis showed that Tb-NTB-BDC crystallizes in the hexagonal $P6_3/mcm$ space group with a = 18.0166 Å, c = 27.4264 Å, V = 7709.8 Å^3, and is formulated as $[(CH_3)_2NH_2]_2[Tb_6(\mu_3\text{-}F)_8(NTB)_2(BDC)_3]{\cdot}x$(solvent). In this structure, the hexanuclear cluster MBB of $[Tb_6(\mu_3\text{-}F)_8(O_2C\text{–})_{12}]$ with S_6 symmetry is fully 12-c. It is noteworthy that the SBL composition in Tb-NTB-BDC is exactly the same as the one in Tb-NTB-HNTB. Nevertheless, the SBLs in Tb-NTB-BDC are stacked on each other in the manner of an eclipsed mode on both sides, in contrast to the slipped one in Tb-NTB-HNTB. The pillars in Tb-NTB-BDC are three fully deprotonated BDC ligands (Fig. 2).

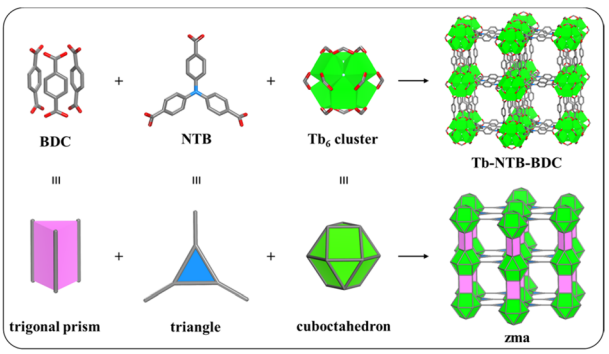

Fig. 2 Top: schematic representation of the structure for Tb-NTB-BDC. Bottom: schematic representation of the topology for Tb-NTB-BDC. Tb = green, C = gray, N = blue, O = red and F = cyan. Hydrogen atoms are omitted for clarity.

Topologically, since the hexanuclear cluster and NTB linker can be deconstructed into cuboctahedron and triangle, and the three BDC ligands connecting both MBBs can be regarded as the three edges of a trigonal prism, the structure was finally analysed as a **zma** network (Fig. 2). In addition, if the inorganic metal cluster and NTB are taken as 8-c and 3-c nodes, and the three triply cross-linked BDC ligands viewed as a linear linker, then Tb-NTB-BDC also exhibits the **tfz** topology that is the same as Tb-NTB-HNTB (Fig. S8†). The formulae for the frameworks of Tb-NTB-1,4-NDC/DTTDC are $[(CH_3)_2NH_2)]_2[Tb_6(\mu_3\text{-}F)_8(NTB)_2(1,4\text{-}NDC)_3(H_2O)_6]{\cdot}x$(solvent) and $[(CH_3)_2NH_2]_2[Tb_6(\mu_3\text{-}F)_8(NTB)_2(DTTDC)_3(H_2O)_6]{\cdot}x$(solvent). In Tb-NTB-BDC/1,4-NDC/DTTDC, there exists the same rhom-

boid one-dimensional channel in the *c*-axis direction associated with the size of 4.00 × 7.72 Å^2, the sizes of rectangular one-dimensional channels along the *a*/*b*-axis are 6.53 × 9.52 Å^2, 3.50 × 9.52 Å^2 and 4.93 × 11.82 Å^2, respectively (Fig. S9†).

For Tb-NTB-OBDC, the SCXRD and ^{19}F NMR[40] analysis (Fig. S1†) show that it crystallizes in the trigonal $P\bar{3}1m$ space group, with cell parameters of a = 18.0964 Å, c = 15.2035 Å, V = 4311.8 Å^3, and is formulated as $[(CH_3)_2NH_2]_2[Tb_6(\mu_3\text{-}F)_8(NTB)_2(OBDC)_3(H_2O)_6]\cdot x$(solvent). In Tb-NTB-OBDC, the hexanuclear cluster MBB of $[Tb_6(\mu_3\text{-}F)_8(O_2C\text{–})_{12}(H_2O)_6]$ is fully 12-c along with C_i symmetry in comparison with S_6 symmetry in Tb-NTB-BDC. Previously identical **kgd** SBLs are formed and stacked against each other in the eclipsed mode. These SBLs are interconnected by OBDC pillars to generate the 3-periodic framework (Fig. 3). It is worth mentioning that each pair of hexanuclear cluster MBBs in Tb-NTB-OBDC, is bridged by only one OBDC linker, which differs from the former structures.

In order to deeply understand the structure, we also use the strategy of merging networks to analyse the topology of the structure. Tb-NTB-OBDC can be deconstructed into two familiar networks. One is the **kgd** network, and the other is a triply interpenetrated topological network, namely **pcu-c3**. The **kgd** network and **pcu-c3** network are merged to obtain a new 3D network with **tpk** topology (**tp** from **pcu-c3**, **k** from **kgd**) (Fig. 3). In addition, if inorganic MBBs are regarded as 12-c nodes, NTB ligands are simplified to 3-c nodes, and OBDC ligands are simplified to connecting rods, Tb-NTB-OBDC is also considered as a new (3,12)-c 3D network (Fig. S11†). Its point symbol (Schläfli symbol) is $\{4^{18}\cdot6^{48}\}$ $2(4^3)$. In this structure, there are two kinds of triangular one-dimensional channels, but their sizes are too small for gas molecules to access the framework through the window.

Characterization

The phase purities of the bulk crystalline materials for Tb-NTB-HNTB, Tb-NTB-BDC, Tb-NTB-1,4-NDC, Tb-NTB-DTTDC and Tb-NTB-OBDC were independently confirmed by the similarities between the calculated and as-synthesized PXRD patterns (Fig. S12†). The thermostability of these pillar-layered MOFs were confirmed by thermal gravimetric analysis (TGA) (Fig. S13†). The solvent accessible free volumes for these compounds were estimated to be 64.0%, 66.6%, 62.9%, 67.6% and 58.7%, by summing voxels more than 1.2 Å away from the framework using PLATON software.[41] To obtain the fully activated framework and further investigate the permanent porosities of these pillar-layered RE-MOFs, Tb-NTB-HNTB was solvent exchanged by acetone for 3 days, Tb-NTB-BDC/1,4-NDC/DTTDC were solvent exchanged by acetone and hexane for 2 h,[42] followed by degassing under high vacuum at 30 °C for 12 h (Tb-NTB-HNTB/DTTDC) or 30 °C for 2 h and 100 °C for 10 h (Tb-NTB-BDC/1,4-NDC) and then loaded onto a gas sorption instrument.

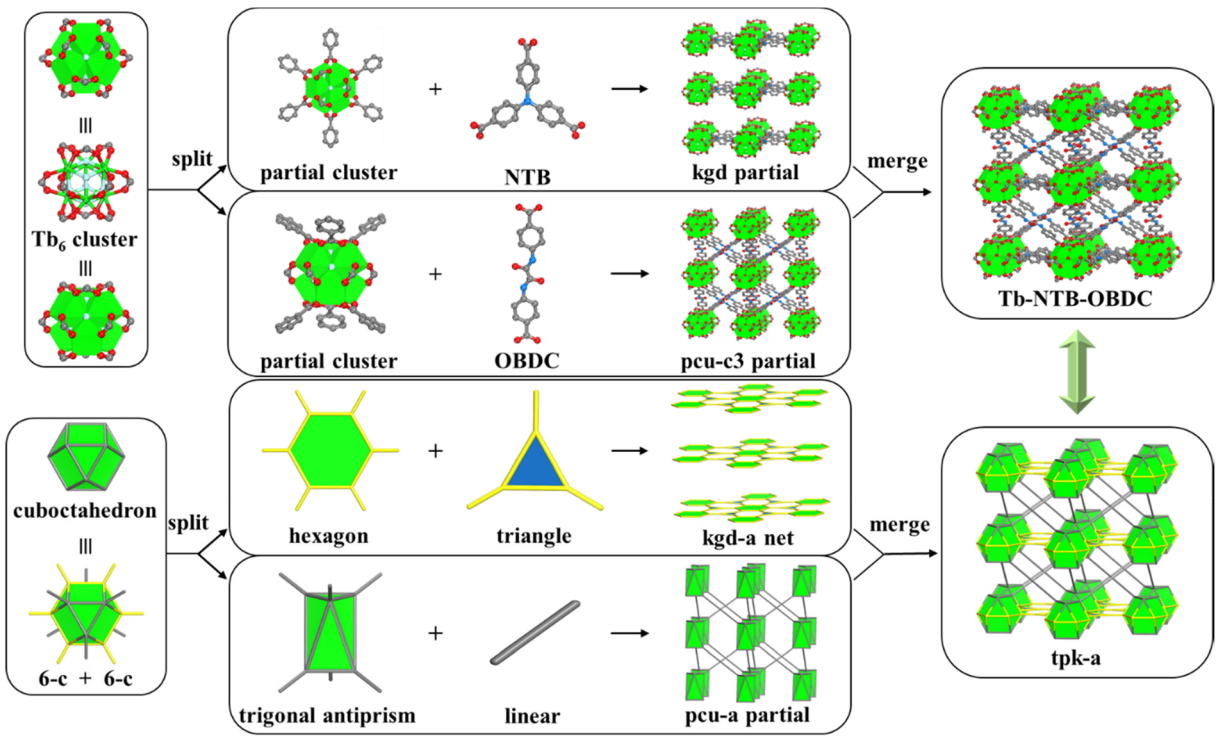

Fig. 3 Schematic representation showing the assembly of Tb-NTB-OBDC. Top: the framework of **kgd** and three interpenetrated **pcu-c3** are combined to form Tb-NTB-OBDC; bottom: **kgd-a** and **pcu-a** nets are merged to form the **tpk-a** network. Tb = green, C = gray, N = blue, O = red and F = cyan. Hydrogen atoms are omitted for clarity.

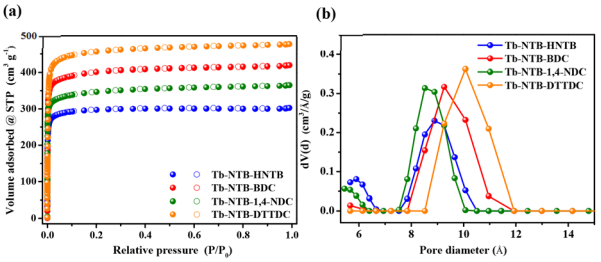

Fig. 4 (a) Nitrogen sorption isotherms at 77 K and (b) pore size distributions of Tb-NTB-HNTB, Tb-NTB-BDC, Tb-NTB-1,4-NDC and Tb-NTB-DTTDC.

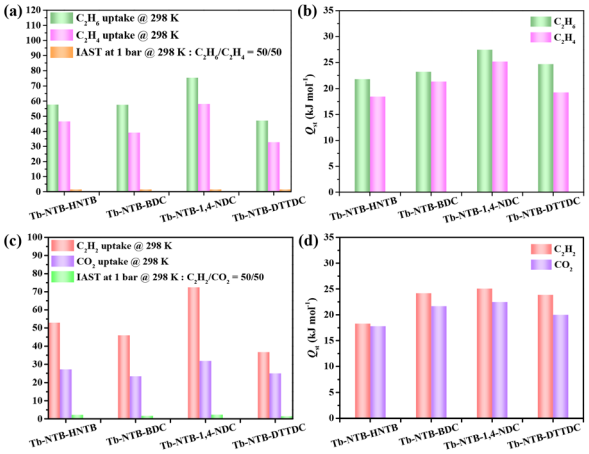

Fig. 5 Uptake and selectivity of (a) C_2H_6 and C_2H_4 and (c) C_2H_2 and CO_2 at 298 K and 1 bar; adsorption enthalpies of (b) C_2H_6 and C_2H_4 and (d) C_2H_2 and CO_2 at zero coverage, for Tb-NTB-HNTB, Tb-NTB-BDC, Tb-NTB-1,4-NDC and Tb-NTB-DTTDC.

As shown in Fig. 4a, all four MOFs display type I N_2 sorption isotherms at 77 K, exclusively representative of microporous features. The apparent BET surface areas and pore volumes were estimated to be 1205 $m^2\ g^{-1}$ and 0.47 $cm^3\ g^{-1}$, 1605 $m^2\ g^{-1}$ and 0.65 $cm^3\ g^{-1}$, 1382 $m^2\ g^{-1}$ and 0.56 $cm^3\ g^{-1}$, 1843 $m^2\ g^{-1}$ and 0.74 $cm^3\ g^{-1}$, respectively, which are close to their theoretical pore volumes. The pore size distributions of Tb-NTB-HNTB range from 5.67 to 6.66 Å and 7.85 to 10.07 Å with widths centered around 5.90 and 8.89 Å; Tb-NTB-BDC ranges from 5.67 to 6.14 Å and 8.52 to 10.96 Å with widths centered around 5.67 and 9.26 Å; Tb-NTB-1,4-NDC ranges from 5.45 to 6.14 Å and 7.53 to 10.07 Å with widths centered around 5.45 and 8.52 Å; Tb-NTB-DTTDC ranges from 9.26 to 10.96 Å with widths centered around 10.07 Å (Fig. 4b), which are in good agreement with their single-crystal analysis data.

C_2H_6/C_2H_4 and C_2H_2/CO_2 adsorption and separation

The four pillar-layered RE-MOFs are characterized by microporous features, with gradually varying pore sizes, and the channels in the structure are enclosed by benzene rings, providing inert pore environments, which prompted us to further investigate their ethane/ethylene as well as acetylene/carbon dioxide separation performances. Firstly, the pure component gas sorption isotherms of C_2H_4 and C_2H_6 for Tb-NTB-HNTB, Tb-NTB-BDC, Tb-NTB-1,4-NDC and Tb-NTB-DTTDC at 273 and 298 K were collected up to 1 bar (Fig. S18 and S19†). The uptake capacities of C_2H_6 and C_2H_4 at 298 K and 1 bar were 57.7, 46.6; 56.7, 39.2; 75.3, 58.1; 47.1, 32.8 $cm^3\ g^{-1}$, respectively (Fig. 5a). It is obvious that all the four materials show the reverse adsorption behaviour between ethylene and ethane, that is, they have the potential to selectively adsorb ethane over ethylene and purify ethylene in a one-step process. Tb-NTB-1,4-NDC shows the highest uptake capacity of C_2H_6 and C_2H_4 among the four materials (Fig. 5a). The zero adsorption enthalpies of C_2H_6 and C_2H_4 for the four materials are 21.8, 18.5; 23.2, 21.4; 27.5, 25.2; 24.7, 19.3 kJ mol^{-1} (Fig. 5b), respectively, which were calculated by the variable temperature adsorption isotherms. The adsorption enthalpy data further indicate that all four materials exhibit stronger affinity for ethane than ethylene, which is consistent with the fact that rich benzene rings tend to form more C–H···π interactions with ethane molecules.[23,24,26] In addition, among the four materials, Tb-NTB-1,4-NDC has the highest adsorption enthalpy for ethane and ethylene, which is also consistent with its highest adsorption amount of ethane and ethylene. Furthermore, the ideal adsorption solution theory (IAST) was used to predict the selectivity of MOF materials under different gas mixture ratios. As shown in Fig. 5a, S20 and S21,† the IAST selectivity of four MOFs was calculated to be *ca.* 1.5 at 298 K and 1 bar. Considering the adsorption capacity and selectivity simultaneously, Tb-NTB-1,4-NDC consequently exhibits the best ethylene/ethane separation potential.

Since the separation of C_2H_2 and CO_2 is of great importance but challenging, pure component adsorption isotherms of C_2H_2 and CO_2 at 273 and 298 K under low pressure for Tb-NTB-HNTB, Tb-NTB-BDC, Tb-NTB-1,4-NDC and Tb-NTB-DTTDC were also collected (Fig. S18 and S19†). The adsorption capacities of C_2H_2 and CO_2 at 298 K and 1 bar were 53.0, 27.2; 46.0, 23.4; 72.5, 31.9; 36.7, 25.0 $cm^3\ g^{-1}$, respectively (Fig. 5c). It can be seen that all four materials exhibit the characteristics of preferentially adsorbing C_2H_2, with Tb-NTB-1,4-NDC showing the highest adsorption capacity of C_2H_2 and CO_2 among the four materials. Furthermore, the IAST selectivity for four MOFs was calculated to be 2.3, 1.8, 2.4, and 1.5 at 298 K and 1 bar, respectively (Fig. 5c, S22 and S23†). Tb-NTB-1,4-NDC possesses the highest C_2H_2/CO_2 IAST selectivity. The zero adsorption enthalpies of C_2H_2 and CO_2 for the four materials are 18.3, 17.3; 24.2, 21.7; 25.1, 22.5; 23.9, 20.0 kJ mol^{-1}, respectively (Fig. 5d), which correlate with their stronger affinity for acetylene than that of carbon dioxide. Finally, Tb-NTB-1,4-NDC also performs best in the selective separation of acetylene and carbon dioxide.

Based on the above studies, combined with the calculation results of single-component gas adsorption capacity, adsorption enthalpy and IAST selectivity, it can be seen that Tb-NTB-1,4-NDC has the best performance among the four materials, regardless of the adsorption and separation poten-

tial of C_2H_6/C_2H_4 or C_2H_2/CO_2. Tb-NTB-1,4-NDC was selected for further tests to verify its practical separation performance. The dynamic column breakthrough experiments were carried out under mixed gas conditions of C_2H_6/C_2H_4 ratios (flow rates) of 25/25 (1 mL min^{-1}) and 5/45 (3 mL min^{-1}), respectively. The experimental results show that C_2H_4 was firstly eluted through the packed bed under different binary gas ratios, without detectable C_2H_6 gas (lower than the detection limit of the thermal conductivity detector), indicating that the reverse adsorption separation of C_2H_4/C_2H_6 can be achieved (Fig. 6a and b). Similarly, we continued to test the breakthrough curves with C_2H_2/CO_2 ratios (flow rates) of 50/50 (1 mL min^{-1}), 50/50 (2 mL min^{-1}), and 50/50 (3 mL min^{-1}) gas mixtures. At the same proportion of different flow rates, CO_2 was eluted through the packed bed firstly, while C_2H_2 continued to remain in the packed bed until it reached a relatively high saturation adsorption capacity and was then eluted (Fig. 7a, b and c), which is consistent with the fact that C_2H_2 has a higher Q_{st} than CO_2. The test results show that Tb-NTB-1,4-NDC can also achieve effective separation of C_2H_2/CO_2. In order to verify the reproducibility of the material performance, we repeated the dynamic breakthrough experiments of C_2H_6/C_2H_4 and C_2H_2/CO_2 at different ratios and flow rates, and the results prove that the material still maintains its separation performance without any loss in the repeat experiments (Fig. 6c, d and 7d–f). It is worth noting that during the repetitive experiments, the regeneration of Tb-NTB-1,4-NDC was carried out under very mild conditions, that is, helium purging at room temperature for only 30 minutes. This further indicates that Tb-NTB-1,4-NDC has great potential for C_2H_6/C_2H_4 and C_2H_2/CO_2 separations.

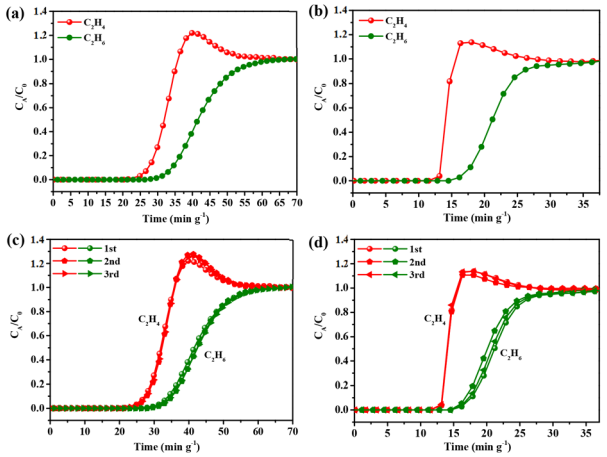

Fig. 6 Experimental column breakthrough curves for (a) C_2H_6/C_2H_4/He (25/25/50) mixture under a flow of 2 mL min^{-1} and (b) C_2H_6/C_2H_4/He (5/45/50) mixtures under a flow of 6 mL min^{-1} in an absorber bed packed with Tb-NTB-1,4-NDC at 298 K and 1.0 bar; (c) and (d) their regenerative tests, respectively.

CH_4 storage

Among the four materials, Tb-NTB-DTTDC has relatively high specific surface area and pore volume, which is suitable for methane storage. At 298 K and 80 bar, the total methane adsorption capacity was 197 cm^3 g^{-1}, and when the temperature was reduced to 273 K, the total methane adsorption capacity increased to 227 cm^3 g^{-1} (Fig. S32†). The methane adsorption capacity of the material at 273 K and 5 bar is 47 cm^3 g^{-1}, which is consistent with its lower zero adsorption enthalpy (*i.e.*, 13.2 kJ mol^{-1}) (Fig. S34†). Thus, the gravimetric

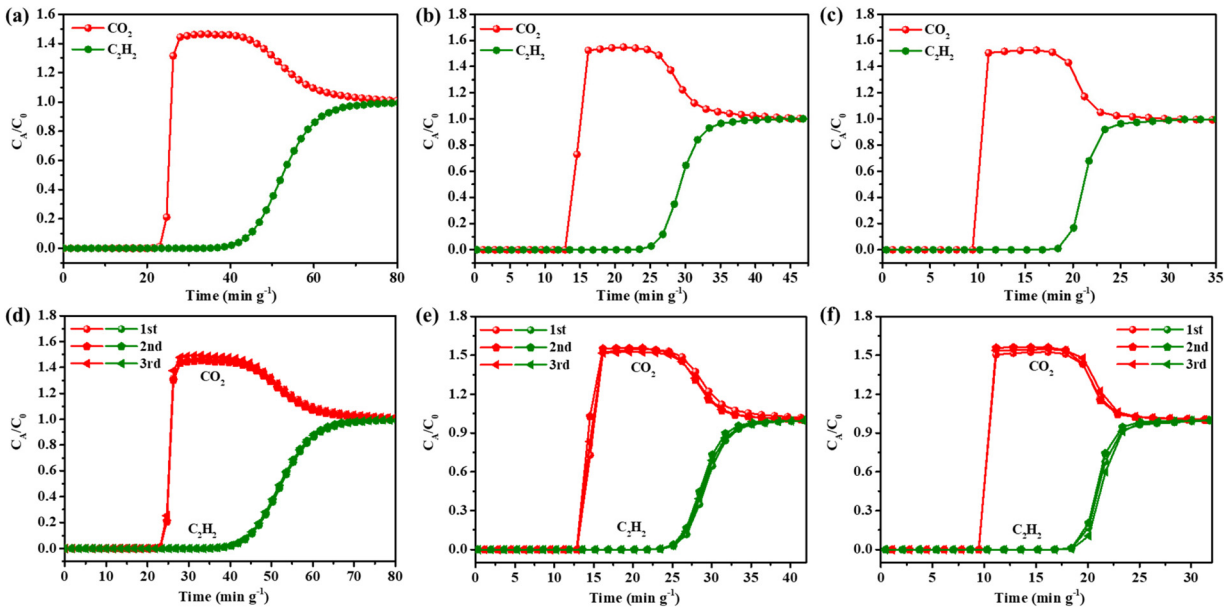

Fig. 7 Experimental column breakthrough curves for (a) C_2H_2/CO_2 (50/50) mixture under a flow of 1 mL min^{-1}, (b) C_2H_2/CO_2 (50/50) mixture under a flow of 2 mL min^{-1} and (c) C_2H_2/CO_2 (50/50) mixture under a flow of 3 mL min^{-1} in an absorber bed packed with Tb-NTB-1,4-NDC at 298 K and 1.0 bar; (d), (e) and (f) their regenerative tests, respectively.

methane storage working capacity of Tb-NTB-DTTDC at 273 K is 180 $cm^3\ g^{-1}$ (0.13 $g\ g^{-1}$).

Conclusions

In summary, five 3D pillar-layered RE-MOFs based on rare **kgd** SBLs were successfully constructed by virtue of rare earth, and sole H_3NTB or mixed dicarboxylic acids, associated with different lengths/functionalities. The Tb_6 clusters and NTB linkers are interconnected to assemble the 2D layer with **kgd** topology in all five structures. Three types of pillar-layered MOFs with different topologies of **trk**, **zma** and **tpk** were identified due to the differences in pillars. More importantly, Tb-NTB-HNTB, Tb-NTB-BDC, Tb-NTB-1,4-NDC and Tb-NTB-DTTDC all exhibit great potential toward C_2H_6/C_2H_4 reverse separation and C_2H_2/CO_2 separation thanks to their microporous features and non-polar pore surfaces. Tb-NTB-1,4-NDC demonstrates the best separation performance among them, and the dynamic breakthrough experiments validated its practical potential for reverse C_2H_6/C_2H_4 separation as well as C_2H_2/CO_2 separation. This work sheds light on rare-earth elements capable for construction of novel pillar-layered MOFs based on rare **kgd** SBLs *via* reticular chemistry *par excellence* toward advanced and systematic applications research.

Author contributions

Hong-Xin Li: investigation, characterization, visualization, writing. Han Fang: visualization. Yu-Feng Zhang: visualization. Zong-Hui Zhang: visualization. Dong-Xu Xue: conceptualization, supervision, writing, funding acquisition.

Conflicts of interest

There are no conflicts to declare.

Acknowledgements

We gratefully acknowledge the National Natural Science Foundation of China (No. 21871170) and the Thousand Talents Program of Shaanxi Province.

References

1 D. S. Sholl and R. P. Lively, Seven chemical separations to change the world, *Nature*, 2016, **532**, 435–437.
2 A. Corma, E. Corresa, Y. Mathieu, L. Sauvanaud, S. Al-Bogami, M. S. Al-Ghrami and A. Bourane, Crude oil to chemicals: Light olefins from crude oil, *Catal. Sci. Technol.*, 2017, **7**, 12–46.
3 J. Y. S. Lin, Molecular sieves for gas separation, *Science*, 2016, **353**, 121–122.
4 S. M. Sadrameli, Thermal/catalytic cracking of hydrocarbons for the production of olefins: A state-of-the-art review I: Thermal cracking review, *Fuel*, 2015, **140**, 102–115.
5 S. M. Sadrameli, Thermal/catalytic cracking of liquid hydrocarbons for the production of olefins: A atate-of-the-art review II: Catalytic cracking review, *Fuel*, 2016, **173**, 285–297.
6 J.-R. Li, R. J. Kuppler and H.-C. Zhou, Selective gas adsorption and separation in metal-organic frameworks, *Chem. Soc. Rev.*, 2009, **38**, 1477–1504.
7 D. J. Safarik and R. B. Eldridge, Olefin/paraffin separations by reactive absorption: A review, *Ind. Eng. Chem. Res.*, 1998, **37**, 2571–2581.
8 T. Ren, M. Patel and K. Blok, Olefins from conventional and heavy feedstocks: Energy use in steam cracking and alternative processes, *Energy*, 2006, **31**, 425–451.
9 M. H. Mohamed, Y. Yang, L. Li, S. Zhang, J. P. Ruffley, A. G. Jarvi, S. Saxena, G. Veser, J. K. Johnson and N. L. Rosi, Designing open metal sites in metal-organic frameworks for paraffin/olefin separations, *J. Am. Chem. Soc.*, 2019, **141**, 13003–13007.
10 F. Jin, E. Lin, T. Wang, S. Geng, T. Wang, W. Liu, F. Xiong, Z. Wang, Y. Chen, P. Cheng and Z. Zhang, Bottom-up synthesis of 8-connected three-dimensional covalent organic frameworks for highly efficient ethylene/ethane separation, *J. Am. Chem. Soc.*, 2022, **144**, 5643–5652.
11 H. Furukawa, K. E. Cordova, M. O'Keeffe and O. M. Yaghi, The chemistry and applications of metal-organic frameworks, *Science*, 2013, **341**, 974–987.
12 J.-R. Li, R. J. Kuppler and H.-C. Zhou, Selective gas adsorption and separation in metal-organic frameworks, *Chem. Soc. Rev.*, 2009, **38**, 1477–1504.
13 R. B. Lin, L. Li, H. L. Zhou, H. Wu, C. He, S. Li, R. Krishna, J. Li, W. Zhou and B. Chen, Molecular sieving of ethylene from ethane using a rigid metal-organic framework, *Nat. Mater.*, 2018, **17**, 1128–1133.
14 C. Gücüyener, J. v. d. Bergh, J. Gascon and F. Kapteijn, Ethane/ethene separation turned on its head: Selective ethane adsorption on the metal-organic framework ZIF-7 through a gate-opening mechanism, *J. Am. Chem. Soc.*, 2010, **132**, 17704–17706.
15 L. Li, R.-B. Lin, R. Krishna, H. Li, S. Xiang, H. Wu, J. Li, W. Zhou and B. Chen, Ethane/ethylene separation in a metal-organic framework with iron-peroxo sites, *Science*, 2018, **362**, 443–446.
16 J. Ploegmakers, S. Japip and K. Nijmeijer, Mixed matrix membranes containing MOFs for ethylene/ethane separation—part B: Effect of Cu_3BTC_2 on membrane transport properties, *J. Membr. Sci.*, 2013, **428**, 331–340.
17 T. M. Nicholson and S. K. Bhatia, Electrostatically mediated specific adsorption of small molecules in metallo-organic frameworks, *J. Phys. Chem. B*, 2006, **110**, 24834–24836.
18 T. M. Nicholson and S. K. Bhatia, Role of electrostatic effects in the pure component and binary adsorption of ethylene and ethane in Cu-tricarboxylate metal-organic frameworks, *Adsorpt. Sci. Technol.*, 2007, **25**, 607–619.

19 Z. Bao, S. Alnemrat, L. Yu, I. Vasiliev, Q. Ren, X. Lu and S. Deng, Adsorption of ethane, ethylene, propane, and propylene on a magnesium-based metal-organic framework, *Langmuir*, 2011, **27**, 13554–13562.

20 E. D. Bloch, W. L. Queen, R. Krishna, J. M. Zadrozny, C. M. Brown and J. R. Long, Hydrocarbon separations in a metal-organic framework with open iron(II) coordination sites, *Science*, 2012, **335**, 1606–1610.

21 S. J. Geier, J. A. Mason, E. D. Bloch, W. L. Queen, M. R. Hudson, C. M. Brown and J. R. Long, Selective adsorption of ethylene over ethane and propylene over propane in the metal-organic frameworks M_2(dobdc) (M = Mg, Mn, Fe, Co, Ni, Zn), *Chem. Sci.*, 2013, **4**, 2054–2061.

22 L. Zhang, L. Li, E. Hu, L. Yang, K. Shao, L. Yao, K. Jiang, Y. Cui, Y. Yang, B. Li, B. Chen and G. Qian, Boosting ethylene/ethane separation within copper(I)-chelated metal-organic frameworks through tailor-made aperture and specific π-complexation, *Adv. Sci.*, 2020, **7**, 1901918–1901924.

23 R. B. Lin, H. Wu, L. Li, X. L. Tang, Z. Li, J. Gao, H. Cui, W. Zhou and B. Chen, Boosting ethane/ethylene separation within isoreticular ultramicroporous metal-organic frameworks, *J. Am. Chem. Soc.*, 2018, **140**, 12940–12946.

24 Z. Di, C. Liu, J. Pang, S. Zou, Z. Ji, F. Hu, C. Chen, D. Yuan, M. Hong and M. Wu, A metal-organic framework with nonpolar pore surfaces for the one-step acquisition of C_2H_4 from a C_2H_4 and C_2H_6 mixture, *Angew. Chem., Int. Ed.*, 2022, **61**, e202210343.

25 L. Guo, M. Savage, J. H. Carter, X. Han, I. da Silva, P. Manuel, S. Rudic, C. C. Tang, S. Yang and M. Schroder, Direct visualization of supramolecular binding and separation of light hydrocarbons in MFM-300(In), *Chem. Mater.*, 2022, **34**, 5698–5705.

26 O. T. Qazvini, R. Babarao, Z. L. Shi, Y. B. Zhang and S. G. Telfer, Robust ethane-trapping metal-organic framework with a high capacity for ethylene purification, *J. Am. Chem. Soc.*, 2019, **141**, 5014–5020.

27 S. Geng, E. Lin, X. Li, W. Liu, T. Wang, Z. Wang, D. Sensharma, S. Darwish, Y. H. Andaloussi, T. Pham, P. Cheng, M. J. Zaworotko, Y. Chen and Z. Zhang, Scalable room-temperature synthesis of highly robust ethane-selective metal-organic frameworks for efficient ethylene purification, *J. Am. Chem. Soc.*, 2021, **143**, 8654–8660.

28 V. Guillerm, D. Kim, J. F. Eubank, R. Luebke, X. Liu, K. Adil, M. S. Lah and M. Eddaoudi, A supermolecular building approach for the design and construction of metal-organic frameworks, *Chem. Soc. Rev.*, 2014, **43**, 6141–6172.

29 J. F. Eubank, H. Mouttaki, A. J. Cairns, Y. Belmabkhout, L. Wojtas, R. Luebke, M. Alkordi and M. Eddaoudi, The quest for modular nanocages: tbo-MOF as an archetype for mutual substitution, functionalization, and expansion of quadrangular pillar building blocks, *J. Am. Chem. Soc.*, 2011, **133**, 14204–14207.

30 S. Yuan, J. S. Qin, L. Zou, Y. P. Chen, X. Wang, Q. Zhang and H. C. Zhou, Thermodynamically guided synthesis of mixed-linker Zr-MOFs with enhanced tunability, *J. Am. Chem. Soc.*, 2016, **138**, 6636–6642.

31 G.-Y. Qiao, S. Yuan, J. Pang, H. Rao, C. T. Lollar, D. Dang, J.-S. Qin, H.-C. Zhou and J. Yu, Functionalization of zirconium-based metal-organic layers with tailored pore environments for heterogeneous catalysis, *Angew. Chem., Int. Ed.*, 2020, **59**, 18224–18228.

32 D.-X. Xue, A. J. Cairns, Y. Belmabkhout, L. Wojtas, Y. Liu, M. H. Alkordi and M. Eddaoudi, Tunable rare-earth fcu-MOFs: A platform for systematic enhancement of CO_2 adsorption energetics and uptake, *J. Am. Chem. Soc.*, 2013, **135**, 7660–7667.

33 D.-X. Xue, Y. Belmabkhout, O. Shekhah, H. Jiang, K. Adil, A. J. Cairns and M. Eddaoudi, Tunable rare earth fcu-MOF platform: Access to adsorption kinetics driven gas/vapor separations via pore size contraction, *J. Am. Chem. Soc.*, 2015, **137**, 5034–5040.

34 V. Guillerm, L. Weselinski, Y. Belmabkhout, A. J. Cairns, V. D'Elia, L. Wojtas, K. Adil and M. Eddaoudi, Discovery and introduction of a (3,18)-connected net as an ideal blueprint for the design of metal-organic frameworks, *Nat. Chem.*, 2014, **6**, 673–680.

35 L. Feng, Y. Wang, K. Zhang, K.-Y. Wang, W. Fan, X. Wang, J. A. Powell, B. Guo, F. Dai, L. Zhang, R. Wang, D. Sun and H.-C. Zhou, Molecular pivot-hinge installation to evolve topology in rare-earth metal-organic frameworks, *Angew. Chem., Int. Ed.*, 2019, **58**, 16682–16690.

36 D. X. Xue, A. Cadiau, L. J. Weselinski, H. Jiang, P. M. Bhatt, A. Shkurenko, L. Wojtas, Z. Chen, Y. Belmabkhout, K. Adil and M. Eddaoudi, Topology meets MOF chemistry for pore-aperture fine tuning: ftw-MOF platform for energy-efficient separations via adsorption kinetics or molecular sieving, *Chem. Commun.*, 2018, **54**, 6404–6407.

37 Y. F. Zhang, Q. Wang, D. X. Xue and J. Bai, Single-crystal synthesis and diverse topologies of hexanuclear Ce(IV)-based metal-organic frameworks, *Inorg. Chem.*, 2020, **59**, 11233–11237.

38 H.-X. Li, Z.-H. Zhang, H. Fang, D.-X. Xue and J. Bai, Synthesis, structure and high methane storage of pure D6R Yb(Y) nonanuclear cluster-based zeolite-like metal-organic frameworks, *J. Mater. Chem. A*, 2022, **10**, 14795–14798.

39 H. Jiang, J. Jia, A. Shkurenko, Z. Chen, K. Adil, Y. Belmabkhout, L. J. Weselinski, A. H. Assen, D. X. Xue, M. O'Keeffe and M. Eddaoudi, Enriching the reticular chemistry repertoire: Merged nets approach for the rational design of intricate mixed-linker metal-organic framework platforms, *J. Am. Chem. Soc.*, 2018, **140**, 8858–8867.

40 J. P. Vizuet, M. L. Mortensen, A. L. Lewis, M. A. Wunch, H. R. Firouzi, G. T. McCandless and K. J. Balkus Jr., Fluoro-bridged clusters in rare-earth metal-organic frameworks, *J. Am. Chem. Soc.*, 2021, **143**, 17995–18000.

41 A. L. Spek, PLATON, *Acta Crystallogr., Sect. A: Found. Crystallogr.*, 1990, **46**, C34.

42 J. Ma, A. P. Kalenak, A. G. Wong-Foy and A. J. Matzger, Rapid guest exchange and ultra-low surface tension solvents optimize metal-organic framework activation, *Angew. Chem., Int. Ed.*, 2017, **56**, 14618–14621.

